Evidence for Filamentarity in the Las Campanas Redshift Survey

Somnath Bharadwaj[a], Varun Sahni[b], B.S. Sathyaprakash[c], Sergei F. Shandarin[d], Capp Yess[e]

[a] Department of Physics and Meteorology, and, Center for Theoretical Studies, I. I. T. Kharagpur 721 302, India

[b]Inter-University Centre for Astronomy & Astrophysics, Post Bag 4, Pune 411007, India

[c]Department of Physics and Astronomy, Cardiff University, Cardiff, CF2 3YB, U.K.

[d]Department of Physics and Astronomy, University of Kansas, Lawrence, KS 66045, USA

Theoretical Astrophysics Center, Copenhagen, Denmark

[e] Department of Physical Sciences, Morehead State University, Morehead, KY 40351-1689, USA

Received _____; accepted _____

ABSTRACT

We apply Shapefinders, statistical measures of 'shape' constructed from two dimensional partial Minkowski functionals, to study the degree of filamentarity in the Las Campanas Redshift Survey (LCRS). In two dimensions, three Minkowski functionals characterise the morphology of an object, they are: its perimeter (L), area (S), and genus. Out of L & S a single dimensionless *Shapefinder Statistic*, $\mathcal{F}$, can be constructed ($0 \leq \mathcal{F} \leq 1$). $\mathcal{F}$ acquires extreme values on a circle ($\mathcal{F} = 0$) and a filament ($\mathcal{F} = 1$). Using $\mathcal{F}$, we quantify the extent of filamentarity in the LCRS by comparing our results with a Poisson distribution with similar geometrical properties and having the same selection function as the survey. Our results unambiguously demonstrate that the LCRS displays a high degree of filamentarity both in the Northern and Southern galactic sections. This is in general agreement with its visual appearence and lends support to the conjecture that the large scale clustering of galaxies is driven by gravitational instability.

Subject headings: Cosmology—galaxies: clustering— large scale structure of the universe: observations–methods: statistical .

1. Introduction

One of the most intriguing features of the galaxy distribution on large scales ($\gtrsim$10Mpc.) is the organisation of matter into geometrically complex structures often described as being cellular, network-like, filamentary, sheet-like, honey-comb etc (Zeldovich, Einasto & Shandarin 1982, Melott 1990, de Lapparent, Geller, & Huchra 1991, Sathyaprakash, Sahni, Shandarin & Fisher 1998). The plethora of adjectives frequently used to qualify the large scale structure of the universe underscores the difficulties inherent in trying to quantify the morphology of the galaxy distribution. This has as much to do with with the need for good robust statistical measures capable of quantifying the geometry and topology of large scale structure as with the virtual absence, until recently, of redshift surveys covering what may be regarded as a truly representative sample of the universe. This last gap in our knowledge has been partially filled with the Las Campanas Redshift Survey (LCRS), which for the first time appears to contain coherent structures whose size is significantly smaller than the survey size. The LCRS may therefore provide us with a statistically unbiased picture of the clustering pattern in the universe on very large scales.

Traditionally, the clustering of galaxies in groups and clusters has been probed with some success by the two point correlation function, $\xi(r)$, which provides an estimate of the probability in excess of random, of finding a galaxy at a distance r from another galaxy. A robust indicator of clustering, the two point correlation function nevertheless reveals very little about the morphology of the galaxy distribution, *i.e.* the concentration of matter in sheets and/or filaments and the geometrical and topological properties of the supercluster-void distribution as a whole. The reason is simple, since $\xi(r)$ is the Fourier transform of the power spectrum $P(k) = \langle|\delta_k|^2\rangle$, it does not describe the build up of phase correlations which lead to the emergence of non-Gaussian features in gravitating systems arising as a result of clustering from Gaussian random initial conditions. Complete

information about clustering is formally contained in the infinite hierarchy of correlation functions ξ_N, $N = 2, 3, ..\infty$. Although attempts have been made to calculate ξ_3 and ξ_4, the presence of a finite number of galaxies in any sample makes the measurement of ξ_N on large scales difficult for large N. Lower order correlation functions must, therefore, be complemented in practise by other statistical measures sensitive to geometry and topology, if we wish to probe the connectedness of large scale structure (and the associated non-Gaussianity) at a more fundamental level.

The first statistical measures to probe the geometry of large scale structure were percolation analysis and the genus curve (Zeldovich 1982, Shandarin 1983, Gott, Melott, & Dickinson 1986). When applied to N-body simulations and galaxy catalogues both methods pick out departures from Gaussianity and are helpful in discerning the presence of 'network-like' and 'sponge-like' features in systems undergoing gravitational clustering. The minimal spanning tree has also proved useful in quantifying geometrical features of large scale structure (Barrow, Bhavsar & Sonoda 1985). More recently, Minkowski functionals have added to our understanding of morphology (Mecke et al. 1994, Schmalzing & Buchert 1997). As demonstrated in Sahni, Sathyaprakash & Shandarin (1998), Shapefinders, a new shape diagnostic constructed out of ratio's of Minkowski functionals, provides valuable information about the 'shape' of a clustering pattern and can be used with considerable advantage (in conjunction with percolation analysis) to study issues relating to the morphology of large scale structure, such as the abundance of sheet-like, filament-like and ribbon-like objects. In the present paper we shall apply Shapefinders to assess the degree of filamentarity in the Las Camapanas Redshift Survey.

The rest of the paper is organized as follows: Sec. 2 defines the statistics we use, Sec. 3 describes the data and the reference cataloges we deal with, finally in Sec. 4 we present our results and conclusions.

2. Minkowski Functionals and the Shapefinder Statistic

In three dimensions, the four Minkowski functionals characterising the morphology of a compact manifold are (Mecke et al. 1994): (i) its volume, V, (ii) surface area, S, (iii) the integrated mean curvature, C, and (iv) the integrated Gaussian curvature, G, (equivalently the Euler characteristic or genus). Percolation analysis can be accomodated within this scheme if one studies the behavior of the volume of the largest cluster as a function of the filling factor for the full cluster distribution (for mass distributions clusters being defined as connected objects lying above a given density threshold). Likewise, the genus curve can be obtained if one plots G as a function of the filling factor. The Shapefinder trio is constructed out of ratio's of Minkowski functionals: $L = \frac{C}{4\pi}$, $W = \frac{S}{C}$, $T = \frac{3V}{S}$. L, W & T have dimensions of length and provide an estimate of physical dimensions of an object such as its *length* L, *width* W and *thickness* T (Sahni, Sathyaprakash & Shandarin 1998). Thus $L \simeq W \simeq T$ characterises a quasispherical cluster, $L \gg W \simeq T$ a filament, $L \simeq W \gg T$ a pancake and $L \gg W \gg T$ a ribbon. Based on L, W, T a pair of dimensionless Shapefinders $\{P, F\}$ can be constructed which provide us with estimates of the planarity $P = \frac{W-T}{W+T}$ and filamentarity $F = \frac{L-W}{L+W}$ of an object, $0 \leq P, F \leq 1$. ($F = P = 0$ for a sphere, $F \simeq 1, P \simeq 0$ for a filament, $F \simeq 0, P \simeq 1$ for a pancake and $F \sim P \sim 1$ for a ribbon.)

In two dimensions the partial Minkowski functionals characterizing the morphology of a connected region are the area S, perimeter L and the number of holes in the region or genus G. The ratio $T = S/L$ characterizes the thickness of the cluster and L its extension. The ratio L/G also has dimensions of length and becomes a meaningful parameter after the onset of percolation, characterizing the scale of the largest cluster; L itself obviously grows unlimitedly with the growth of the survey size.

It appears that the Shapefinder statistic is a much better diagnostic of shape than moment-based methods, particularly when applied to topologically complex bodies such as

isodensity surfaces occuring at moderate density thresholds in N-body simulations and in galaxy catalogues (Sathyaprakash, Sahni & Shandarin 1998).

In two dimensions, the Shapefinder statistic simplifies to a *single number*

$$\mathcal{F} = \frac{L^2 - 4\pi S}{L^2 + 4\pi S} \tag{1}$$

where L is the perimeter and S the area of a closed two dimensional contour. (This could be an isodensity contour in a two dimensional galaxy distribution, an isotherm of a hot/cold spot in a map of the Cosmic Microwave Background (Novikov, Feldman & Shandarin 1999), etc.) By definition $0 \leq \mathcal{F} \leq 1$; $\mathcal{F} \simeq 1$ for an ideal filament (having a finite length and zero width), and $\mathcal{F} \simeq 0$ for a circular disc.

The Las Campanas Redshift Survey contains redshifts of about 25,000 galaxies making it the largest magnitude limited three-dimensional catalogue of galaxies to date. However, the six slices into which LCRS is divided are all quasi-two-dimensional, which makes the two-dimensional shapefinder $\mathcal{F}$ appropriate for its study.

Before applying the Shapefinder statistic to discern filamentary features in the LCRS, we shall first demonstrate its effectiveness by determining $\mathcal{F}$ for certain eikonal shapes in two dimensions. The first object whose shape we study is an ellipse of semi-major axis a, semi-minor axis b and eccentricity $\epsilon = \sqrt{1 - b^2/a^2}$. The area of such an ellipse is

$$S = \pi a b \tag{2}$$

and its perimeter is given by

$$L = 4a \int_0^{\pi/2} \sqrt{1 - \epsilon^2 \sin^2\theta}\, d\theta \tag{3}$$

(A reasonable approximation to (3) is provided by $L \simeq 2\pi\sqrt{\frac{a^2+b^2}{2}}$.) In table 1 we show the value of $\mathcal{F}$ as the ellipse is gradually deformed from an initially circular shape to a highly filamentary final shape. As pointed out in Sahni, Sathyaprakash & Shandarin (1998)

other Shapefinders can also be constructed out of the Minkowski functionals S and L, a good example being provided by the transformations $\mathcal{F}' = \mathcal{F}^p$ and $\mathcal{F}'' = \sin(\pi\mathcal{F}/2)$ which define new Shapefinders from the canonical form (1). Transformations such as these can be made to define statistics that are in conformity with the visual impression of morphology of archetypal structures.

In table 1, we show results for $\mathcal{F}$, $\mathcal{F}'$ (with $p = 1/2$) and $\mathcal{F}''$. From the results presented in this Table, we see that the Shapefinder family $\mathcal{F}$, $\mathcal{F}'$ and $\mathcal{F}''$ acquires continuous values between 0 and 1 as a circle is deformed into a filament, and that filamentarity is more accentuated in $\mathcal{F}'$ and $\mathcal{F}''$ than in $\mathcal{F}$. It is interesting to contrast the behaviour of $\mathcal{F}$ with that of the eccentricity, ϵ, another parameter characterising shape but defined *only* for an ellipse. While the value of $\mathcal{F}$ grows in proportion to the deformation of the ellipse (and is therefore reflective of the latter's visual shape), the change in ϵ is sudden, with the result that ϵ rapidly approaches unity even for relatively small deformations of the ellipse. Although the eccentricity is extremely good for measuring the small deviations from a circle it is clearly not the kind of behaviour one wishes to see in a 'well behaved' shape-statistic which should also be sensitive to large deviations from a circle.

Next, we examine a *topologically non-trivial* object – the region between two concentric circles with radii R_1 and R_2, $R_2 \leq R_1$ (circular disc-with-a-hole). In this case:

$$S = \pi(R_1^2 - R_2^2), \qquad L = 2\pi(R_1 + R_2), \tag{4}$$

and the expression for $\mathcal{F}$ turns out to be very simple

$$\mathcal{F} = \frac{R_2}{R_1}. \tag{5}$$

As the radius of the hole R_2 shrinks to zero, the object becomes a circular disc with $\mathcal{F} \simeq 0$, in the other extreme case when $R_1 \sim R_2$ the disc-with-a-hole reduces to a circular filament having $\mathcal{F} \simeq 1$ (rather like the mythological serpent eating its tail). One should note that

the presence of circular symmetry would lead a moment-based statistic to wrongly declare such an object as being circular or homogeneous (Sathyaprakash, Sahni & Shandarin 1998).

Results of increasing the hole size by increasing R_2 are shown in Table 2 for $\mathcal{F}$, $\mathcal{F}'$ and $\mathcal{F}''$. They are in broad agreement with those obtained earlier for the ellipse. We therefore find that the two dimensional Shapefinder statistic gives sensible results when applied to both simple and topologically complicated eikonal shapes. This conclusion is supported by results obtained for three dimensional Shapefinders by Sahni et al. (1998) and Sathyaprakash, Sahni & Shandarin (1998). In this paper we shall apply $\mathcal{F}$ to study filamentarity in the Las Camapanas Redshift Survey (the results of applying $\mathcal{F}'$ and $\mathcal{F}''$ are qualitatively similar and will not be discussed separately).

3. Analysis.

3.1. The Las Camapanas Redshift Survey.

The Las Camapanas Redshift Survey (LCRS) contains approximately 25,000 galaxies with known redshifts. The survey region is divided into six slices, three each in the Northern (N_1, N_2, N_3) and Southern (S_1, S_2, S_3) Galactic hemispheres. The slices are strips of the sky 1.5° thick and 80° wide which are separated by 3° and probe a distance of up to 600 h^{-1}Mpc. (h is the value of the Hubble parameter in units of 100 km $sec^{-1}Mpc^{-1}$). The centers of the three northern slices are at declinations −3° (N_1), −6° (N_2) and −12° (N_3), whereas the three southern slices are centered at −39° (S_1), −42° (S_2) and −45° (S_3). The survey is complete to limiting magnitude $m = 17.75$ (for more details of the LCRS survey see Shectman et al 1996).

In order to minimise selection and projection effects we apply the Shapefinder statistic to a volume limited subsample of the LCRS derived from the dense central region

Table 1: Shapefinders $\mathcal{F}$, $\mathcal{F}'$ & $\mathcal{F}''$ describe the shape of an ellipse having semi-major axis a, semi-minor axis b and eccentricity ϵ.

a/b	ϵ	$\mathcal{F}$	$\mathcal{F}' = \mathcal{F}^{1/2}$	$\mathcal{F}'' = \sin(\pi\mathcal{F}/2)$
1	0	0	0	0
3	0.94	0.20	0.45	0.31
5	0.98	0.38	0.62	0.56
10	0.99	0.61	0.78	0.82

Table 2: Shapefinders $\mathcal{F}$, $\mathcal{F}'$ & $\mathcal{F}''$ describe the shape of the region between two concentric circles with radii R_1 & R_2 (circular disc-with-a-hole).

R_1, R_2	$\mathcal{F}$	$\mathcal{F}' = \mathcal{F}^{1/2}$	$\mathcal{F}'' = \sin(\pi\mathcal{F}/2)$
10, 0	0	0	0
10, 2	0.20	0.45	0.31
10, 4	0.40	0.63	0.59
10, 6	0.60	0.77	0.81
10, 8	0.80	0.89	0.95
10, 9	0.90	0.95	0.99

$200 \leq R \leq 400$ h^{-1} Mpc. (The LCRS selection function peaks at $R \simeq 200$ h^{-1}Mpc. and the region $200 \leq R \leq 400$ h^{-1} Mpc corresponds to the densest part of the survey.) In order to ascertain the statistical significance of our results we compare them with a statistically homogeneous two-dimensional Poisson distribution with identical selection function and geometry as the survey and corrected for projection effects (for more details, see Shandarin & Yess 1998).

Each slice is embedded in a 560×260 grid with resolution 1 h^{-1}Mpc. This enables us to define galaxy locations on a two dimensional lattice. Lattice cells containing a galaxy are said to be occupied or *filled*, and lattice cells with no galaxies are referred to as *empty*. The cells which lie outside the boundaries of the survey are eliminated from the lattice.

Next, we proceed to 'grow' structure (or coarse-grain) by means of the following iterative procedure: At each step filled cells are made to grow isotropically (*i.e.* in all directions) by a single unit of the mesh size. Thus any cell neighboring a filled cell (one containing a galaxy) in any of eight possible directions is also designated 'filled'. This algorithm leads to the growth of filled cells at each successive iteration.

The procedure of sequentially coarse-graining a LCRS slice is shown in Figure 1 for the N1 slice. Incidentally, it also visualizes what happens when the size of the dots in the wedge diagram plots are arbitrarily chosen. Selecting the size of the dots or the linking length one can emphasize 'desired' features of the distribution such as filamentarity, connectivity, the size of the greatest supercluster or something else. So far no reason has been suggested in the literature for a particular choice of the linking length (except one corresponding to percolation transition) and therefore we use it or actually the size of the dots for the purpose of parameterization.

The associated *filling factor* (FF), defined as the fraction of filled cells in the total slice, increases from a small initial value to almost unity when all the cells in the LCRS slice have

inter-connected into one big all-pervading cluster. At any given value of FF (*i.e.* at any given iterative step) we determine clusters using a friends-of-friends algorithm: any filled cell sharing a common side with another filled cell is its friend. All such 'friends' define a cluster. The shape of individual clusters defined in this manner can be analysed using the Shapefinder statistic at different values of the filling factor. Large scale connectedness of galaxies in LCRS is also revealed by studying the Largest Cluster Statistics (LCS) characterizing the percolation transition as a function of the filling factor (LCS is defined as the ratio of the area of the largest cluster to the total area of all clusters, see Shandarin & Yess 1998).

3.2. Shapefinders on a grid

The Shapefinders (1) were defined for continuous contours. For contours on a grid this definition must be modified. It is easy to see that the lattice version of (1) is

$$\mathcal{F}_1 = \frac{L^2 - 16S}{L^2 + 16S} \tag{6}$$

(Note that the factor 4π in (1) has been replaced by 16 in (6).) Consider a rectangle defined on a grid with sides $n \times l$ and $m \times l$, respectively, where l is the inter-grid spacing. It is easy to see that in this case $\mathcal{F}_1$ reduces to

$$\mathcal{F}_1 = \frac{(n-m)^2}{(n+m)^2 + 4nm} \tag{7}$$

as a result $\mathcal{F}_1 = 0$ for $n = m$ (a square), and $\mathcal{F}_1 \to 1$ for $n \gg m$ (a filament).

It is interesting that one can define a second Shapefinder statistic which is also suitable for determining shapes of contour lines defined on a grid. Again, if l is the inter-grid spacing we have

$$\mathcal{F}_2 = \frac{L^2 - 16S}{(L - 4l)^2} \tag{8}$$

so that, for the rectangle (n, m)

$$\mathcal{F}_2 = \frac{(n-m)^2}{(n+m-2)^2}. \tag{9}$$

We see that once more $\mathcal{F}_2 = 0$ for $n = m$ (a square), and $\mathcal{F}_2 \to 1$ for $n \gg m$ (a filament). A specific feature of $\mathcal{F}_2$ is that a rectangular contour of unit width $(n, 1)$ is always delared to be a filament regardless of its length n, since, substituting $m = 1$ in (9) we get $\mathcal{F}_2 = (n-1)^2/(n-1)^2 = 1$.

One might question the need for introducing two separate statistics to study shapes on a lattice. The reason for this is related to the following question: Consider an 'ideal' one-dimensional filament having a finite length but zero breadth. How would one go about representing this object on a grid ? Depending upon how one answers this question one arrives at either $\mathcal{F}_1$ or $\mathcal{F}_2$. One might argue that the discrete analogue of an ideal filament would be a rectangular object with width $\sim l$, (*i.e.* width = mesh size) in which case $\mathcal{F}_2$ gives the correct continuum limit: $\mathcal{F}_2 = \mathcal{F} = 1$. On the other hand one might equally argue that a filament having width $< l$ is impossible to correctly define on a grid for which the Nyquist wavelength determines an effective small scale 'resolution cutoff'. Therefore, if one is confined to a grid one must necessarily differentiate between objects having identical widths $(\sim l)$ but varying in length, in this case the correct statistic to use is $\mathcal{F}_1$.

In this paper, we report on work carried out using both $\mathcal{F}_1$ and $\mathcal{F}_2$. As we shall show, $\mathcal{F}_1$ and $\mathcal{F}_2$ contain complementary information about filamentarity, as a result both prove to be very useful shape-diagnostics for large scale structure.

Novikov, Feldman & Shandarin 1999 used yet another approach to measuring the Minkowski functionals on a grid. Studying the 4-year COBE maps they assumed a smooth underlying field and, therefore, used a linear interpolation scheme for measuring the perimeters and areas of the clusters.

The largest cluster in two dimensions can be characterized by two parameters: the wall thickness $T = S/L$ and the length of the boundary per one void L/G. The perimeter itself L is not a good measure because it obviously diverges as the area of the survey grows unlimitedly. On the other hand the parameter L/G defined for the percolating cluster proves to be remarkably stable over a wide range of linking lengths. Fig. 5 shows the length of the boundary per void (L/G) as a function of the thickness (S/L) for both the LCRS and reference catalogues. The stability of L/G is is reflected bythe fact that while the thickness grows from $\approx$ 5Mpc to $\approx$ 16Mpc the mean value of L/G decreases only marginally: from $\approx$ 110Mpc to $\approx$ 70Mpc in the LCRS catalogue. (The structure in the reference Poisson catalogues is of considerably smaller size than in the LCRS.)

4. Results and Conclusions.

In Figures 2 and 3, we show the extent of filamentarity as a function of the filling factor for three northern and three southern slices of LCRS (the volume limited slice contain from 800 to 1,600 galaxies). The extent of filamentarity is quantified using an area weighted filamentarity statistic, $F_{1,2}$ [1], constructed out of either $\mathcal{F}_1$ or $\mathcal{F}_2$:

$$F_{1,2} = \frac{\sum_i S_i^2 \mathcal{F}_{1,2}^i}{\sum_i S_i^2}, \qquad 0 \leq F_{1,2} \leq 1. \tag{10}$$

Here S_i is the area and $\mathcal{F}_{1,2}^i$ the filamentarity of the i^{th} cluster. (Each cluster is identified using a nearest neighbors algorithm at a given value of the coarse-graining.)

The sum is over all clusters in the slice. The statistic $F_{1,2}$ is designed to receive proportionally greater weight from more massive clusters since we believe larger clusters

[1]Here we reduce statistical information present in the distribution function by computing the weighted mean values.

provide a greater contribution to the perceived filamentarity of LCRS. To assess the statistical significance of our results we compare $F_{1,2}$ with the corresponding quantity derived from four independent Poisson randomizations of the given LCRS slice. From Figures 2 and 3 it is clear that for moderate values of the filling factor the extent of filamentarity in *all* six slices of LCRS is *significantly greater* than in the Poisson sample. This is true for both $\mathcal{F}_1$ and $\mathcal{F}_2$. Comparing Fig. 2 (obtained using $\mathcal{F}_1$) with Fig. 3 (obtained using $\mathcal{F}_2$) we find that the difference between LCRS and the Poisson sample shows up at much lower filling factors for $\mathcal{F}_2$. The reason for this is simple, as we demonstrated earlier, $\mathcal{F}_2$ is designed to be more successful in picking out smaller filaments than $\mathcal{F}_1$. At low FF, small filaments appear to be much more abundant in LCRS than they are in the Poisson sample, as a result $\mathcal{F}_2$ easily discerns filamentarity in LCRS at small FF. Together $\mathcal{F}_1$ and $\mathcal{F}_2$ probe the extent of filamentarity over a wide range of FF. We should mention that we have also studied the extent of filamentarity in LCRS using other 'moments' of the Shapefinder statistic $\mathcal{F}$ such as: $F_{1,2}^{(p)} = \frac{\sum_i S_i^p \mathcal{F}_{1,2}^i}{\sum_i S_i^p}$. Since our results are in broad qualitative agreement with those shown in figures 2 and 3 for $p = 2$, we do not consider it necessary to discuss them separately in this paper.

Complementary information emphasising the 'connectivity' of a distribution is revealed by percolation analysis (Shandarin & Yess 1998). At small FF each slice contains a large number of distinct clusters whose shape must be determined individually. As the FF increases, neighboring clusters begin to merge leading to a decrease in the total number of clusters in the sample and to the emergence of a single dominant 'supercluster'. With increased FF we find that the largest cluster shows a very rapid increase in size as a result of which it soon spans the entire survey region. This corresponds to the onset of percolation. We determine $\mathcal{F}$ for individual clusters and FF of the largest cluster at each level of coarse graining. As $FF \rightarrow 1$ the percolating supercluster fills the entire slice, the value of $\mathcal{F}$ then drops to a small value which describes the shape of the survey region. (If the slice were an

exact square the value $\mathcal{F}$ would approach 0 as $FF \rightarrow 1$.) In Fig. 4 we plot the Largest Cluster Statistic (LCS is the fractional size of the largest cluster relative to all clusters at a given value of coarse graining) against FF (the fraction of filled cells in the total area of the slice). Comparing these results with those of the Poisson distribution we clearly see that the growth in the largest cluster is more rapid in LCRS than it is in the randomized catalogue (constructed with the same selection function and number of galaxies and therefore having identical geometrical properties to LCRS) confirming the earlier results of Shandarin and Yess (1998).

To summarise we have shown that clustering of galaxies in LCRS is significantly non-Gaussian: it is dominated by filaments and its global geometry is network-like (in the parlance of Shandarin & Yess 1998). Our analysis also indicates that Shapefinders recognize non-Gaussian features in LCRS at lower filling factors than the percolation curve and that Shapefinders and percolation analysis supplement each other in discerning the geometrical properties of the galaxy distribution on large scales.

Finally we note that at $FF \sim 1$ the extent of filamentarity in LCRS declines (from a value close to unity) and becomes smaller than in the Poisson catalogue. The decrease in F in both LCRS and the Poisson catalogue is simply due to the fact that all clusters in the sample have now merged into a single 'superduper cluster' which resembles a quasi-homogeneous object with several holes (empty regions). Such an object when probed using the Shapefinder statistic appears very filamentary both in LCRS and the Poisson sample. However as $FF \rightarrow 1$ the holes gradually get filled and F drops to a small value which describes the shape of the survey region. We do not attach significance to results obtained at $FF > 0.6$ because at large FF (significantly after the percolation transition) the coarse - grained distribution ceases to resemble the underlying galaxy sample from which it was constructed.

Fig. 5 gives the scale of the structure, however we wish to stress that it is not the diameter of the empty cells seen in Fig. 1. The parameter L/G has a meaning of 'length of the contour line per void'. In our case the mean number of voids is large: about 30 in the LCRS and about 130 in the randomized catalogues (at thickness $\approx$ 10Mpc). This allows us to say that the sample is sufficiently large and the average diameter of the voids (at thickness $\approx$ 10Mpc) is about $80/\pi \approx 25$Mpc.

It is interesting to note that an analysis of LCRS using the genus curve has shown that at large values of the smoothing radius, LCRS reveals statistical properties which are consistent with those of a Gaussian random field (Colley 1997). Our results on the other hand (and those of Shandarin & Yess 1998) show that the *unsmoothed* LCRS catalogue displays strongly non-Gaussian features. In this context, it is worthwhile to reiterate that N-body gravitating systems clustering from Gaussian initial conditions rapidly develop non-Gaussian features reflected both in a network-like structure and by a growth of filamentarity in the morphology of clusters and superclusters (Sathyaprakash, Sahni & Shandarin 1996, Sahni, Sathyaprakash & Shandarin 1997, Sathyaprakash, Sahni & Shandarin 1998). The effects of smoothing such a distribution on large scales would be to add greater weight to the clustering of long range modes still in the linear regime, and hence statistically distributed in the manner of a Gaussian random field (Dominik & Shandarin 1992, Sahni & Coles 1995). When viewed in this context the results of this paper (and those of Shandarin & Yess 1998), together with the results of Colley (1997), appear to provide strong support for the scenario in which the large scale structure of the universe evolved via gravitational clustering from Gaussian initial conditions predicted (for instance) by Inflationary Models of the very early universe.

Acknowledgements. S. Shandarin acknowledges the support of NSF-EPSCoR grant, GRF grant at the University of Kansas and from TAC Copenhagen.

REFERENCES

Barrow, J.D., Bhavsar, S.P. & Sonoda D.H. 1985, MNRAS **216**, 17.

Colley, W.N. 1997, ApJ **489**, 471.

de Lapparent, V., Geller, M.J. & Huchra, J.P. 1991, ApJ, **369**, 273.

Dominik, K. & Shandarin, S.F. 1992, ApJ, **393**, 450.

Gott, J.R., Melott, A.L. & Dickinson, M. 1986, ApJ, **306**, 341.

Mecke, K.R., Buchert, T. & Wagner, H., 1994, Astron. Astrophys., **288**, 697.

Melott, A.L. 1990, Physics Reports, **193**, 1.

Novikov, D.I., Feldman, H. & Shandarin, S.F. 1999, International Journal of Modern Phys. D, **8**, No 3, to be published, astro-ph/9809238

Sahni, V. & Coles, P., 1995, Physics Reports, **262**, 1.

Sahni, V., Sathyaprakash, B.S. & Shandarin, S.F. 1997, ApJ **476**, L1.

Sahni, V., Sathyaprakash, B.S. & Shandarin, S.F. 1998, ApJ **495**, L5.

Sathyaprakash, B.S., Sahni, V. & Shandarin, S.F. 1996, ApJ, **462**, L5.

Sathyaprakash, B.S., Sahni, V., Shandarin, S.F. and Fisher, K. 1998, ApJ, **507**, L109.

Sathyaprakash, B.S., Sahni, V. & Shandarin, S.F. 1998, ApJ **508**, 551.

Schmalzing, J. & Buchert, T. 1997, ApJ **482**, L1.

Shandarin, S.F. 1983, Soviet Astron. Lett., **9**, 104.

Shandarin, S. and Yess, C. 1998, ApJ, **505**, 12.

Shectman, S.A., Landay, S.D., Oemler, A., Tucker, D.L., Kirshner, R.P., Lin, H. and Schechter, P.L. 1996, *Wide-Field Spectroscopy and the Distant Universe, Proceedings of the 35th Herstmonceux Conference*, eds. S.J. Maddox and A. Aragon-Salamanca, World Scientific, Singapore.

Zeldovich, Ya. B. 1982, Soviet Astron. Lett., **8**, 102.

Zeldovich, Ya. B., Einasto, J. & Shandarin, S.F. 1982, Nature, **300**, 407.

This manuscript was prepared with the AAS LaTeX macros v4.0.

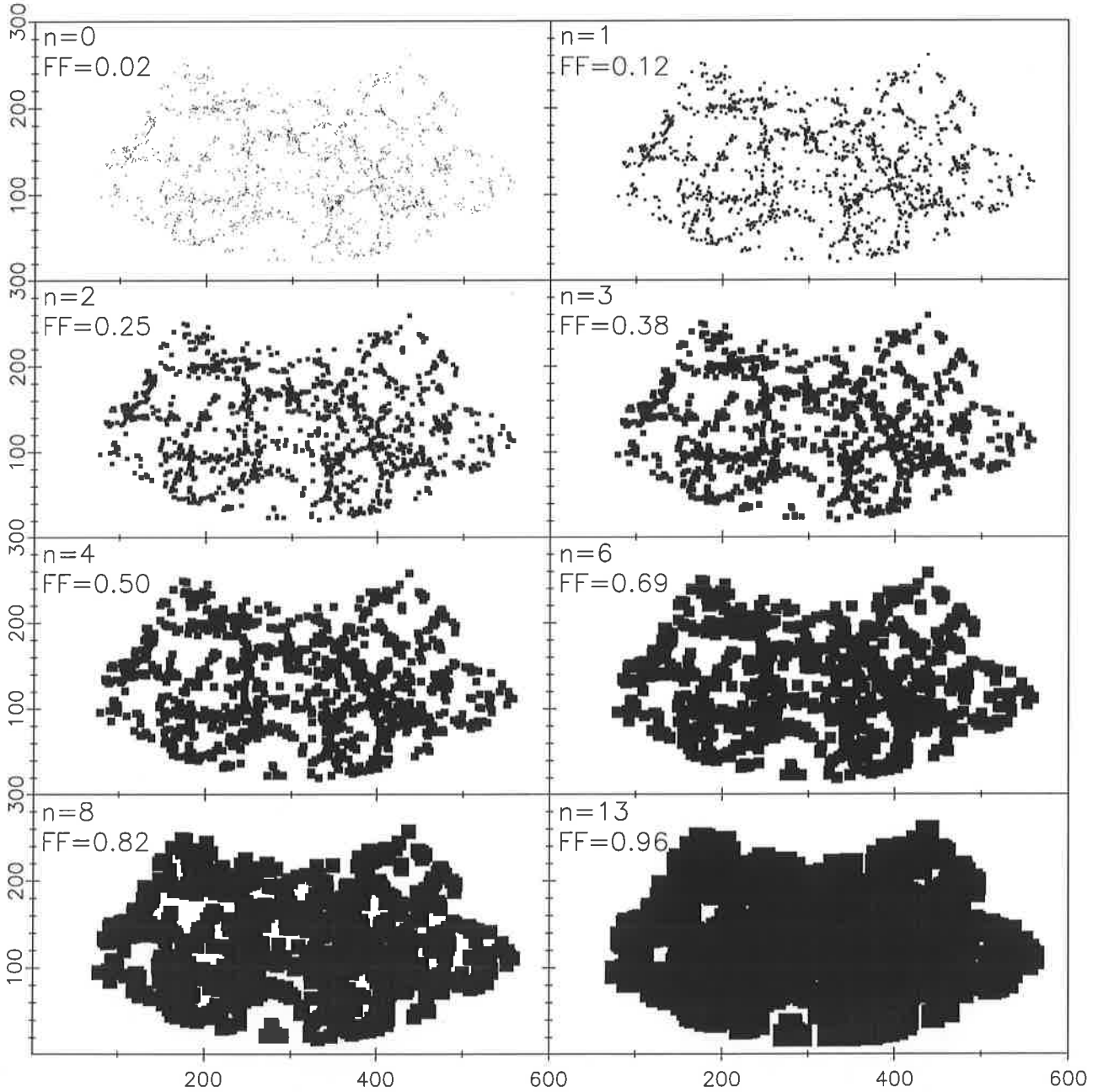

Fig. 1.— The first Northern LCRS slice shown at different values of coarse-graining (n). The value of the filling factor (FF) at each level of coarse-graining is also shown. Here n = 0 shows galaxies in the original N_1 slice without coarse graining. The axis units are h^{-1} Mpc.

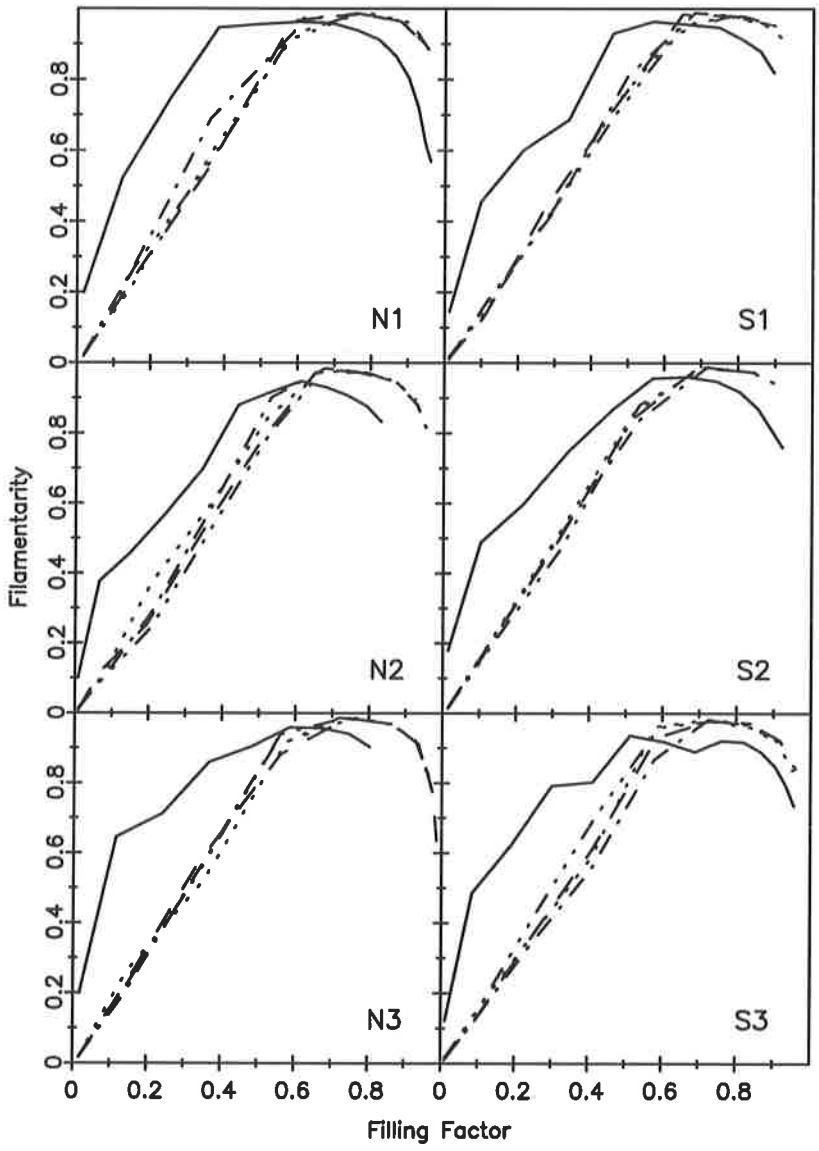

Fig. 2.— The filamentarity statistic F is shown plotted against the filling factor FF for each slice in the LCRS (solid line). For comparison we also show F for four independent random realizations of each of the slices (dashed and dotted lines). The shape-statistic F shown here is constructed from the discrete Shapefinder $\mathcal{F}_1$.

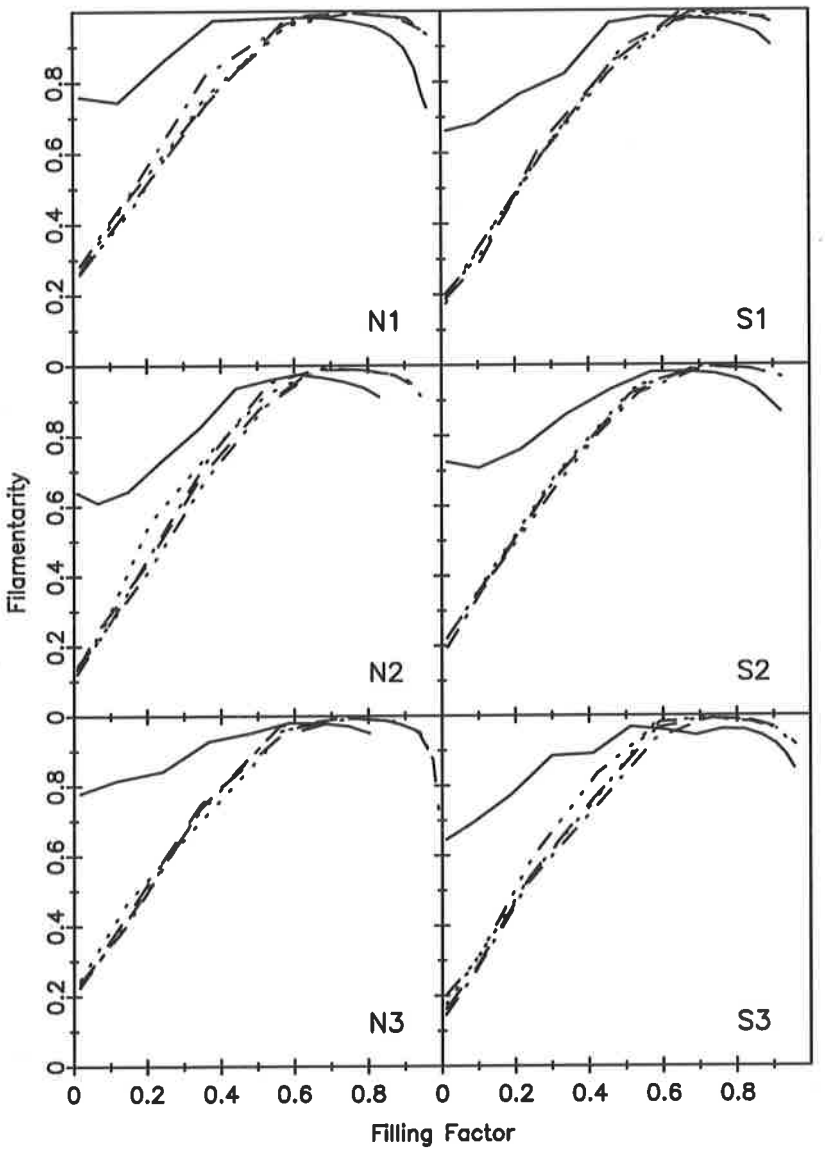

Fig. 3.— The filamentarity statistic F is shown plotted against the filling factor FF for each slice in the LCRS (solid line). For comparison we also show F for four independent random realizations of each of the slices (dashed,dotted lines). The shape-statistic F shown here is constructed from the discrete Shapefinder $\mathcal{F}_2$.

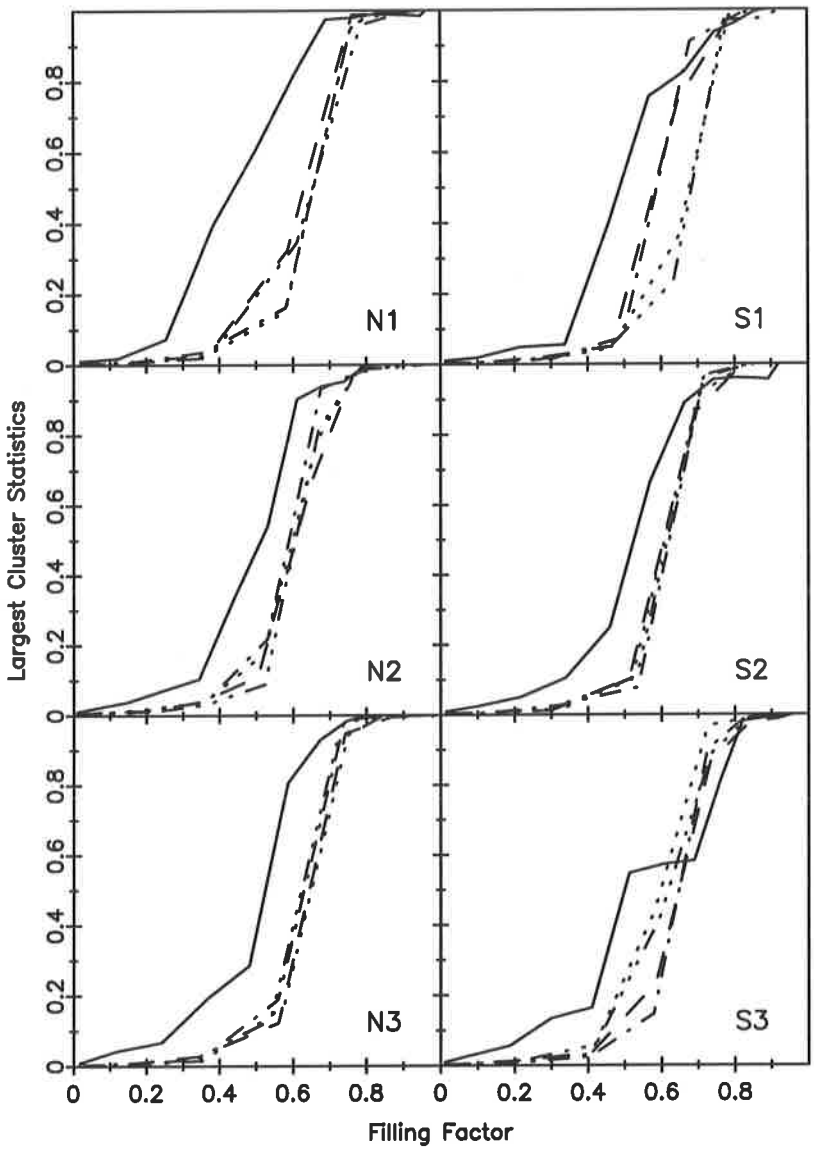

Fig. 4.— The largest cluster statistics (LCS) is shown plotted against the filling factor FF for each slice in the LCRS (solid line). For comparison we also show (LCS) for four independent random realizations of each of the slices (dashed,dotted lines).

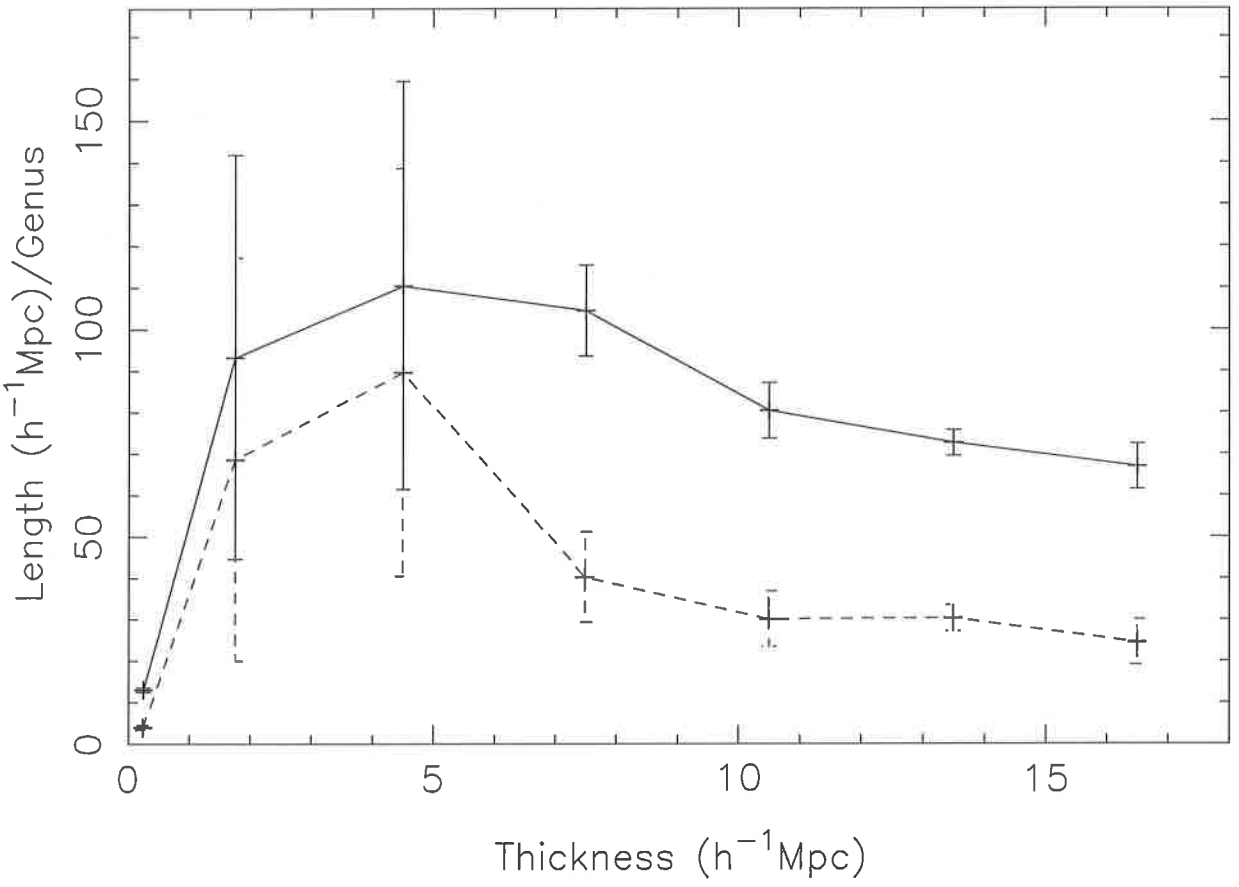

Fig. 5.— The solid curve shows the ratio length/genus of the largest cluster plotted as a function of the thickness of the largest cluster. The values of the thickness from the different slices have been divided into bins of $3h^{-1}$ Mpc and the average value of the length/genus in each bin has been plotted as the solid curve. The error-bars show $1-\sigma$ fluctuations. For comparison we have shown the same quantity for the random catalogues using dashed lines.